AEM
Journals.ASM.org

Geochemical Niches of Iron-Oxidizing Acidophiles in Acidic Coal Mine Drainage

Daniel S. Jones,[a]* Courtney Kohl,[a] Christen Grettenberger,[a] Lance N. Larson,[b]* William D. Burgos,[b] Jennifer L. Macalady[a]

Department of Geosciences, Penn State University, University Park, Pennsylvania, USA[a]; Department of Civil and Environmental Engineering, Penn State University, University Park, Pennsylvania, USA[b]

A legacy of coal mining in the Appalachians has provided a unique opportunity to study the ecological niches of iron-oxidizing microorganisms. Mine-impacted, anoxic groundwater with high dissolved-metal concentrations emerges at springs and seeps associated with iron oxide mounds and deposits. These deposits are colonized by iron-oxidizing microorganisms that in some cases efficiently remove most of the dissolved iron at low pH, making subsequent treatment of the polluted stream water less expensive. We used full-cycle rRNA methods to describe the composition of sediment communities at two geochemically similar acidic discharges, Upper and Lower Red Eyes in Somerset County, PA, USA. The dominant microorganisms at both discharges were acidophilic *Gallionella*-like organisms, "*Ferrovum*" spp., and *Acidithiobacillus* spp. *Archaea* and *Leptospirillum* spp. accounted for less than 2% of cells. The distribution of microorganisms at the two sites could be best explained by a combination of iron(II) concentration and pH. Populations of the *Gallionella*-like organisms were restricted to locations with pH >3 and iron(II) concentration of >4 mM, while *Acidithiobacillus* spp. were restricted to pH <3 and iron(II) concentration of <4 mM. *Ferrovum* spp. were present at low levels in most samples but dominated sediment communities at pH <3 and iron(II) concentration of >4 mM. Our findings offer a predictive framework that could prove useful for describing the distribution of microorganisms in acid mine drainage, based on readily accessible geochemical parameters.

Acid mine drainage (AMD) is the low-pH, iron-rich discharge that occurs when pyrite (FeS_2) and other metal sulfide minerals in ore deposits or coal seams are exposed to atmospheric conditions by mining activity. AMD impacts over 10,000 km of streams in the Appalachian region of the United States alone, and the cost for AMD treatment worldwide may exceed US$100 billion using existing technologies (1–3). Widely applied treatment strategies include active and passive systems designed to accelerate iron oxidation and removal by raising the pH of the waste stream to circumneutral values (4). However, iron removal may also be achieved at low pH by promoting biological iron oxidation by acidophilic microorganisms. Low-pH biological iron oxidation might enhance existing passive treatment technologies or be developed for novel alternative bioremediation strategies (5, 6).

AMD generation by the oxidation of pyrite can be described with four reactions. Pyrite is initially oxidized by oxygen (equation 1) or Fe^{3+} (equation 2), which produces acid and Fe^{2+} ions.

$$FeS_2 + H_2O + \tfrac{7}{2}O_2 \rightarrow Fe^{2+} + 2SO_4^{2-} + 2H^+ \quad (1)$$

$$FeS_2 + 8H_2O + 14Fe^{3+} \rightarrow 15Fe^{2+} + 2SO_4^{2-} + 16H^+ \quad (2)$$

Fe^{2+} is subsequently oxidized to Fe^{3+} (equation 3), which may precipitate as iron oxyhydroxide minerals (equation 4) or act as an electron acceptor for further pyrite oxidation (equation 2).

$$Fe^{2+} + \tfrac{1}{4}O_2 + H^+ \rightarrow Fe^{3+} + \tfrac{1}{2}H_2O \quad (3)$$

$$Fe^{3+} + 3H_2O \rightarrow Fe(OH)_3 + 3H^+ \quad (4)$$

All four reactions can occur when the pyrite-bearing formation is exposed to oxygen, but iron oxidation and precipitation by equations 3 and 4 can continue to drive down pH values long after the discharge has been removed from the pyrite source, as is the case in many Appalachian coal mine drainages (for an example, see reference 7). Iron is removed from solution by oxidation and Fe oxide precipitation, but the abiotic oxidation of Fe^{2+} is very slow at pH values of <4 (8). Iron-oxidizing acidophiles can overcome this kinetic barrier and promote equation 3 even under extremely acidic conditions, and thus they can play an important catalytic role in low-pH AMD treatment.

Specific iron oxidation rates for acidophilic isolates range from 192 to 532 mg min^{-1} g $protein^{-1}$ for autotrophic strains and from 191 to 449 mg min^{-1} g $protein^{-1}$ for heterotrophic strains (9). When different isolates were used to treat real and synthetic AMD in packed-bed bioreactors, a betaproteobacterial isolate (later named "*Ferrovum myxofaciens*" [10]) achieved the fastest iron oxidation rates while *Acidithiobacillus ferrooxidans* proceeded the slowest (11). Microbial communities that develop naturally in AMD sediments also have different iron oxidation capabilities. In experiments with sediments from the Lower Red Eyes coal mine

Received 8 September 2014 **Accepted** 4 December 2014

Accepted manuscript posted online 12 December 2014

Citation Jones DS, Kohl C, Grettenberger C, Larson LN, Burgos WD, Macalady JL. 2015. Geochemical niches of iron-oxidizing acidophiles in acidic coal mine drainage. Appl Environ Microbiol 81:1242–1250. doi:10.1128/AEM.02919-14.

Editor: G. Voordouw

Address correspondence to Daniel S. Jones, dsjones@umn.edu, or Jennifer L. Macalady, jlm80@psu.edu.

* Present address: Daniel S. Jones, Department of Earth Sciences and BioTechnology Institute, University of Minnesota, Minneapolis, Minnesota, USA; Lance N. Larson, Natural Resources Defense Council, Washington, DC, USA.

Supplemental material for this article may be found at http://dx.doi.org/10.1128/AEM.02919-14.

doi:10.1128/AEM.02919-14

drainage in Pennsylvania, USA, cell-normalized iron oxidation rates were nearly twice as fast in reactors incubated with *Ferrovum*-dominated sediments as with *Acidithiobacillus*-dominated sediments (7). In a subsequent study, cell-normalized iron oxidation rates determined for AMD sediments from multiple drainages with different microbial assemblages varied by up to 7 times (12). Thus, identifying and selecting for specific Fe-oxidizing populations may improve the efficiency and effectiveness of low-pH bioremediation systems (for an example, see reference 6).

Although diverse acidophilic iron-oxidizing organisms have been identified over the past several decades, relatively little is known about what factors control their occurrence and distribution in nature. pH seems to be especially important for controlling microbial distribution in AMD (for examples, see references 13 and 14). For example, a recent analysis of 59 AMD sites in China found that pH was the most important explanatory variable across all sites (15). However, many taxa co-occur in similar pH ranges, and other studies have found that environmental factors, including dissolved oxygen, conductivity, temperature, and iron and other metal concentrations are also important controls on microbial community composition (14–20). In addition to contemporary environmental selection, microbial populations may also be affected by geographic isolation, which can maintain microbial communities independent of contemporary environmental factors by preserving the influence of past environmental factors or the history of stochastic microbial colonization (19, 21).

In this study, we quantified microbial taxa across a geochemical gradient in two AMD springs, Upper Red Eyes (URE) and Lower Red Eyes (LRE), Pennsylvania, USA. Previous work at Lower Red Eyes showed that sediment microbial communities change with distance across the mound and that distinct sediment communities exhibited different cell-normalized iron oxidation rates (7). In order to identify which variables controlled the distribution of acidophiles at Upper and Lower Red Eyes, we performed a detailed analysis of microbial communities in and downstream from the two discharges, including seasonal changes. We found that the distribution of the three most abundant populations could best be explained by a combination of pH and $[Fe^{2+}]$.

MATERIALS AND METHODS

Field sampling and geochemistry. Upper Red Eyes and Lower Red Eyes drainages are located approximately 500 m apart in Somerset County, PA (URE, lat 40.2410, long −78.7407; LRE, lat 40.2402, long −78.7467). The AMD-impacted water at both locations is sourced from boreholes that channel underground drainage from nearby abandoned coal mines (7). The iron oxide mounds produced by the drainages form a series of stepped pools and terraces as described in reference 7. Water flow is slow in pools and rapid in areas where it cascades over vertical drops created by the terraces. The geochemistry of the sites is described in references 7 and 12.

We collected surface sediment and water samples in 2009 and 2011 at multiple locations along transects downstream from the springs. Samples for DNA extraction were immediately frozen in the field on dry ice and stored at −80°C until analysis. Samples for fluorescent *in situ* hybridization (FISH) were fixed in 4% paraformaldehyde as described previously (22). Temperature, conductivity, dissolved oxygen, pH, and oxidation-reduction potential (ORP) were measured in the field using handheld meters (WTW, Weilheim, Germany; Oakton Instruments, IL, USA; or Beckman Coulter, CA, USA). Water samples for iron and trace metal analyses were filtered (0.2 μM) in the field and preserved with concentrated HCl and HNO_3, respectively. Total and ferrous iron were measured by the ferrozine assay (23), sulfate was measured by barium sulfate precipitation (Hach method 8051), and cations, total sulfur, and trace metals were analyzed by inductively coupled plasma atomic emission spectroscopy (ICP-AES) at the Penn State Materials Characterization Laboratory.

Field ORP values measured against the standard calomel electrode were converted to standard hydrogen electrode (E_H) values as described in reference 24 and converted to p*e* according to the relationship $pe = FE_H/2.303RT$, where F is Faraday's constant (C mol^{-1}), R is the gas constant (J mol^{-1} K^{-1}), and T is temperature (K). ORP values were measured only at URE, so we calculated p*e* at LRE from the activities of Fe^{2+} and Fe^{3+} according to the relationship $pe = pe^o - \log(\{Fe^{3+}\}/\{Fe^{2+}\})$, where pe^o is the empirically determined value at standard state (13 for the reaction $Fe^{3+} + e- \rightarrow Fe^{2+}$ [25]) and braces denote activity. Activity coefficients for Fe^{2+} and Fe^{3+} were calculated using the Davies equation (26). Ionic strength was calculated from specific conductivity values as in reference 27, using the average specific conductivities for URE and LRE (2.3 and 4.5 mS cm^{-1}, respectively). p*e* values from ORP field measurements at URE were in good agreement with calculated values from $\{Fe^{3+}\}/\{Fe^{2+}\}$, except at the emergent spring, where oxygen was below detection and no Fe^{3+} was detectable ($r^2 = 0.78$, excluding values from the emergence) (see Fig. S1 in the supplemental material).

DNA extraction and 16S rRNA gene sequencing. DNA was extracted from Red Eyes sediment samples as described in reference 28, after removing iron by repeated ammonium oxalate washes as described in reference 29. Environmental 16S rRNA genes were cloned from LRE sediment samples LRE21 and LRE22, collected on 28 July 2009 from 10.4 and 26.8 m downstream from the LRE emergence, respectively. Cloning of sample LRE22 was described and reported in reference 7, and cloning of sample LRE21 was performed as for LRE22, using bacterial primers 27f and 1492r as described in references 7 and 28. Clones were end sequenced at the Penn State Core Genomics Facility (ABI Hitachi 3730XL DNA analyzer with BigDye fluorescent terminator chemistry). An amplicon library was generated from sample LRE21 DNA extracts by pyrosequencing the hypervariable V6 region of the 16S rRNA gene. Amplification, barcoding, and pyrosequencing (GS-FLX platform; Roche, Switzerland) were performed at the Marine Biological Laboratory (Woods Hole, MA) as described by McCliment et al. (30). Sequences were deposited in GenBank as indicated below.

FISH and probe design. Fluorescence *in situ* hybridization of AMD sediments was performed as described in reference 7. FISH probes and competitor oligonucleotides (31) used in this study are listed in Table 1. The design and optimization of FISH probe FERRI643 were described in reference 7. We designed a new FISH probe (GAL177) to target the genus *Gallionella* and all *Gallionella*-like sequences retrieved from the study sites. We optimized GAL177 by testing a range of formamide stringencies from 0 to 45%, using a pure culture of *Acidithiobacillus thiooxidans* as a negative control (1 nucleotide mismatch) and an environmental sample from the site where LRE21 was obtained as a positive control (which contained *Gallionella*-like organisms according to cloning). To ensure specificity of GAL177, we designed two competitor oligonucleotides (31), GAL177c1 and GAL177c2 (Table 1). The competitors bind to 1-mismatch sequences at probe position 14, which represent more than 95% of the 1-mismatch hits in our ARB database. The use of the competitors in an equimolar mixture with GAL177 consistently resulted in no visible signal from the 1-mismatch negative-control cells at 20% formamide stringency. The widely used FISH probes for *Betaproteobacteria* (BET42a) and *Gammaproteobacteria* (GAM42a) do not bind specifically to those clades (32). BET42a hits over 92% of the betaproteobacterial sequences but also 7% of the gammaproteobacterial sequences in a 23S rRNA gene database (Silva LSU ref database, version 115 [33]). Together, however, these two probes hit over 92% of the *Gamma-* and *Betaproteobacteria*, with only three mismatches outside these groups. As it is now widely recognized that the *Betaproteobacteria* form a subgroup within the *Gammaproteobacteria* in rRNA gene phylogenies (34), we combined GAM42a and BET42a in an equimolar mixture (GAMBET) to target both groups (Table 1).

TABLE 1 Fluorescence *in situ* hybridization probes used in this study

Probe name[a]	Sequence (5′–3′)	% formamide	Specificity	Label	Reference or source
EUB338	GCT GCC TCC CGT AGG AGT	0–50	Most *Bacteria*	FITC	54
EUB338-II	GCA GCC ACC CGT AGG TGT	0–50	*Planctomycetales*	FITC	55
EUB338-III	GCT GCC ACC CGT AGG TGT	0–50	*Verrucomicrobiales*	FITC	55
ARCH915	GTG CTC CCC CGC CAA TTC CT	20	Most *Archaea*	CY3	56
THIO1	GCG CTT TCT GGG GTC TGC	35	*Acidithiobacillus* spp.	CY3, CY5	57
FERRI643	ACA GAC TCT AGC TTG CCA	35	*Ferrovum* spp.	CY3	11
Gal177	TCC CCC TCA GGG CAT A	20	*Gallionella* spp.	CY3	This study
Gal177c1	TCC CCC TCA GGG CTT A		Competitor for Gal177		This study
Gal177c2	TCC CCC TCA GGG CGT A		Competitor for Gal177		This study
LF655	CGC TTC CCT CTC CCA GCC T	35	*Leptospirillum* spp.	CY3	58
BET42a	GCC TTC CCA CTT CGT TT	35	Most *Betaproteobacteria*, some *Gammaproteobacteria*	CY3	59
GAM42a	GCC TTC CCA CAT CGT TT	35	Most *Gammaproteobacteria*	CY3	59

[a] EUBMIX is a mixture of EUB338, EUB338-II; and EUB338-III, GAMBET is a mixture of GAM42a and BET42a; GAM42a and BET42a target the 23S rRNA sequence. All other probes target the 16S rRNA sequence.

FISH was performed on multiwell Teflon-coated glass slides, mounted with Vectashield (Vector Laboratories, CA, USA), viewed with a Nikon Eclipse 80i epifluorescence microscope, and photographed with a monochrome Photometrics Coolsnap ES2 charge-coupled-device (CCD) camera and NIS-Elements AS 3.0 software. The abundances of probe-labeled cells were obtained by counting at least 400 DAPI (4′,6-diamidino-2-phenylindole)-stained cells for each sample-and-probe combination. The means and standard deviations were calculated from counts of at least 8 microscope fields and at least two slide wells.

Phylogenetic, diversity, and other statistical analyses. Nearly full-length 16S rRNA gene clones were quality checked and assembled with CodonCode Aligner version 1.2.4 (CodonCode Corp., United States) and manually checked for ambiguities. Sequences were aligned to the 7,682-character Hugenholtz alignment using the NAST aligner at Greengenes (35). Clones were checked for chimeric sequences with Bellerophon 3 (36), and putative chimeras were removed. NAST-aligned sequences were loaded into an ARB database (37) containing over 500,000 nearly full-length sequences (base database downloaded from Greengenes [35] in May 2011). Alignments were manually refined using the ARB_Edit4 sequence editor. Prior to phylogenetic analyses, alignments were end clipped to remove missing data, and positions with >50% gaps were filtered from the alignment (final alignment, 1,383 positions for the analysis of *Gallionellaceae*). Phylogenic analyses included the top BLAST matches to each sequence in GenBank and their closest relatives in our ARB database. Neighbor-joining analyses were performed in PAUP* v. 4b10 (38) with Jukes-Cantor-corrected distances and 2,000 bootstrap replicates.

The LRE21 V6 amplicon library was uploaded to VAMPS (http://vamps.mbl.edu) and quality screened using the default VAMPS pipeline. Taxonomic assignments were performed using GAST software (39) and a 16S rRNA V6 reference database available at http://vamps.mbl.edu. Representative sequences for operational taxonomic units (OTUs) were extracted using mothur (40), and taxonomic assignments were confirmed by BLASTN analysis (41) against the Silva 16S rRNA sequence database (33).

Nonmetric multidimensional scaling (NMDS), canonical correspondence analyses (CCA), and other statistical analyses were performed using the vegan package (42) in R (43). Population data based on FISH were input as the average proportion of the total DAPI-stained cells labeled by each probe, as described above. Statistical analyses included the following two "other" categories: "other" *Gamma-* and *Betaproteobacteria* [GAMBET − (FERRI643 + GAL177 + THIO1)] and "other" bacteria (EUBMIX − GAMBET). Prior to ordination analyses, environmental parameters were standardized to maximum values. Mantel tests (44) were performed in R using Bray-Curtis distance matrices and 999 permu-

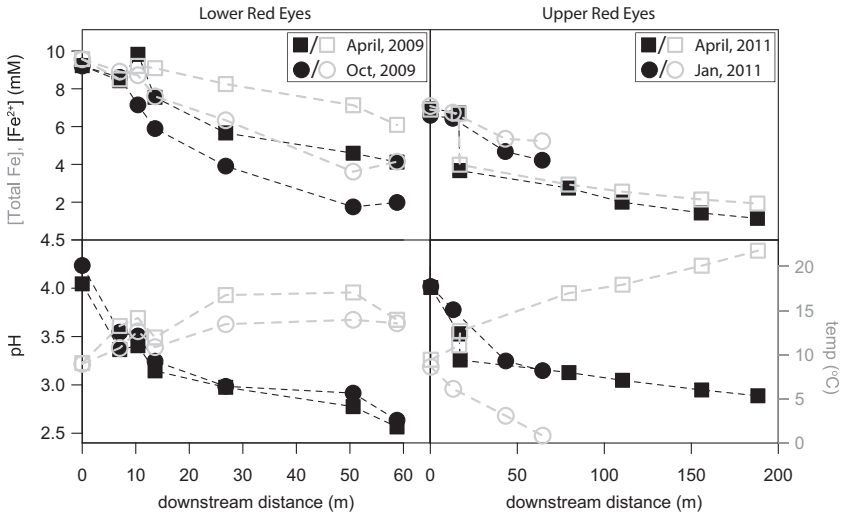

FIG 1 Changes in [Fe^{2+}] (black, top), total [Fe] (gray, top), pH (black, bottom), and temperature (gray, bottom) with distance at Lower and Upper Red Eyes. The geochemical data from Lower Red Eyes from April 2009 were reported in reference 7.

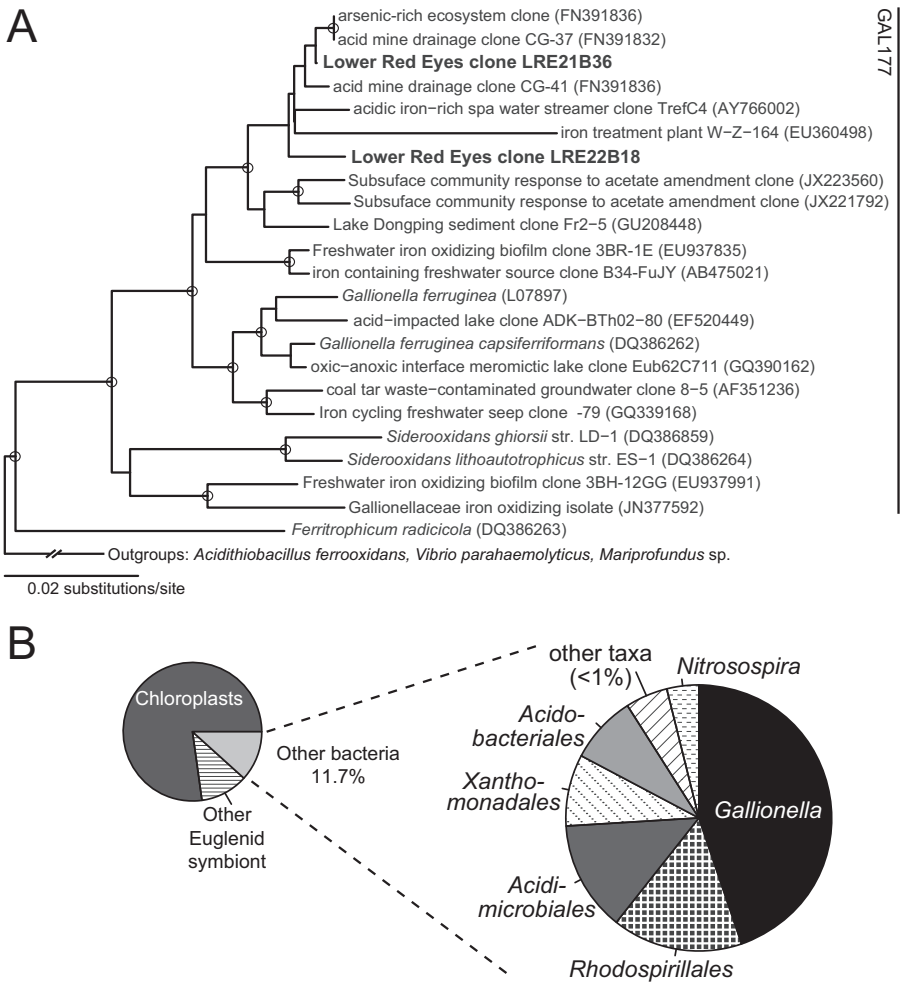

FIG 2 (A) Neighbor joining phylogram of the *Gallionellaceae*, including the *Gallionella*-like sequences from Red Eyes. Open circles indicate nodes supported by >90% bootstrap support. (B) Community composition of sample LRE21 based on pyrotag sequencing of the V6 region of 16S rRNA gene.

tations, with environmental parameters standardized by column maximum. Communities sampled from terrace sediments were compared to communities from the corresponding pool sample at LRE sites (indicated in Table S1 in the supplemental material) by analysis of similarities (ANOSIM) (44).

Nucleotide sequence accession numbers. Nearly full-length 16S rRNA gene clone sequences from Red Eyes were deposited in GenBank under accession numbers HQ420110 to HQ420152 and KM488364 to KM488407. The V6 amplicon library is available in VAMPS (http://vamps.mbl.edu) under the id LRE09_21_Bv6.

RESULTS

Field observations and geochemistry. Upper and Lower Red Eyes drainages (URE and LRE) originate from anoxic springs with pH values between 4.0 and 4.5 and Fe^{2+} concentrations in excess of 6.5 mM (Fig. 1). Downstream from the springs, pH values and both Fe^{2+} and total Fe concentrations decreased with distance. Downstream pH trends were generally consistent at different times of the year, but trends in water temperature and total Fe and Fe^{2+} differed according to season (Fig. 1). Sulfate decreased slightly downstream (see Fig. S2 in the supplemental material) (7). Dissolved oxygen was below detection at the emergent springs and approached saturation at all downstream sites (7, 12). In January 2011, thick ice prevented further downstream sampling at URE. Trace metal concentrations remained constant downstream at both sites (reported for LRE in reference 7 and for URE in reference 12).

Iron precipitates at URE and LRE form mounds characterized by stepped pools and terraces. Near the springs, iron-rich orange sediments were colonized by green benthic biofilms characteristic of the algae *Euglena* spp., which disappeared downstream. In stagnant pools, iron oxide mineral precipitates exposed at the sediment-water interface were generally uncemented and easy to disturb. Well-cemented iron oxide precipitates were associated with water cascading over terrace rims. Iron oxide sediments at Red Eyes often display a "cauliflower" morphology characteristic of schwertmannite, $Fe_8O_8(OH)_6(SO_4)\cdot nH_2O$, consistent with the dominant mineralogy at the site as reported in reference 7.

16S rRNA gene sequencing. We cloned 43 nonchimeric 16S rRNA gene sequences from sample LRE21 (10.4 m downstream of emergence). In previous work (7), 44 nonchimeric 16S rRNA gene clones were retrieved from sample LRE22 (26.8 m downstream of emergence). The most abundant phylotype in sample LRE22 (47% of clones) grouped with the genus *Ferrovum* in the *Betaproteobacteria* (see Fig. 5 in reference 7). Other taxa in the LRE22

clone library include relatives of *Acidimicrobium* spp. in the *Actinobacteria* (19%), as well as *Acidobacteria* (2%), chloroplasts (5%), and other *Beta-*, *Alpha-*, and *Gammaproteobacteria* (12%, 7%, and 7%, respectively) (7). In contrast, the majority of sequences (84%) from LRE21 were >99% similar to chloroplasts of the algae *Euglena mutabilis*, and 12.5% were most closely related to a proteobacterial symbiont of another euglenid, *Trachelomonas scabra* strain NJ T235. The remaining clone from LRE21 was from a sister group to the clade containing isolates of the neutrophilic iron-oxidizing genus *Gallionella* (Fig. 2A). For deeper characterization of sample LRE21, we created an amplicon library of the hypervariable V6 region of the 16S rRNA gene. We obtained 5,694 amplicons from sample LRE21, of which 77.2% were putative chloroplast sequences and 11.1% were mostly closely related to the same *Trachelomonas* sequence as above. The remaining 11.7% were from other bacteria, presumably representing the free-living bacterial community. Forty-two percent of those sequences were assigned to the *Gallionellaceae* family, which includes the genus *Gallionella* and the single LRE21 clone (Fig. 2B).

The closest sequenced relatives to Red Eyes *Gallionellaceae* clones LRE21B36 and LRE22B18 (Fig. 2A) are environmental sequences from an acidic, iron-rich spa (45) and from an AMD treatment plant (46). These sequences form a sister group to the clade containing *Gallionella ferruginea* and environmental sequences from circumneutral iron-rich freshwater springs (Fig. 2A). We refer to the acidophilic Red Eyes organisms as "*Gallionella*-like" or *Gallionellaceae* because they are closely related to but phylogenetically distinct from described *Gallionella* spp. The *Gallionella*-like organisms at Red Eyes and their closest relatives occur in acidic (pH 3 to 4), oxygenated streams (see also references 45 and 46), in contrast to the micro-oxic, circumneutral habitat of *Gallionella ferruginea* and other *Gallionella* spp. (47).

Red Eyes sediment communities. Over 80% of prokaryotic cells in all samples stained with the *Bacteria*-specific probe EUBMIX (Fig. 3; see also Table S1 in the supplemental material). Most samples were dominated by the *Gamma-* and *Betaproteobacteria* (probe GAMBET), except those from the October transect at LRE, which had >40% other bacteria at all sites (Fig. 3B). The only other samples with <60% *Gamma-* or *Betaproteobacteria* included those from the emergent pool at LRE, which was dominated by bacteria with spirochete morphology (not shown), and the furthest downstream sites at URE, in which the proportion of *Gamma-* and *Betaproteobacteria* decreases with downstream distance (Fig. 3D).

Probes for the *Gallionellaceae* family (GAL177) and bacterial genera *Acidithiobacillus* (THIO1) and *Ferrovum* (FERRI653) each labeled over 80% of the cells in at least one sample (Fig. 4; see also Table S1 in the supplemental material). Probes for *Archaea* (ARCH915) and for the bacterial genus *Leptospirillum* (LF655) hybridized with less than 2% of cells in all samples. The relative abundance of THIO1-, FERRI653-, and GAL177-labeled cells changed downstream, with GAL177-positive cells generally most abundant near the springs, followed by FERRI643-positive cells, and finally THIO1-positive cells at some downstream sites (Fig. 3). Most samples contained over 5% FERRI643-positive cells, while GAL177- and THIO1-positive cells were absent from many samples (see Table S1 in the supplemental material). THIO1-positive cells were abundant at downstream LRE sites (far from the spring) but never made up more than 3% of cells at URE. Groups present in rRNA gene libraries that we did not target using specific FISH probes include *Xanthomonadales* (*Gammaproteobacteria*), *Acidimicrobium* (*Actinobacteria*), and *Rhodospirillales* (*Alphaproteobacteria*).

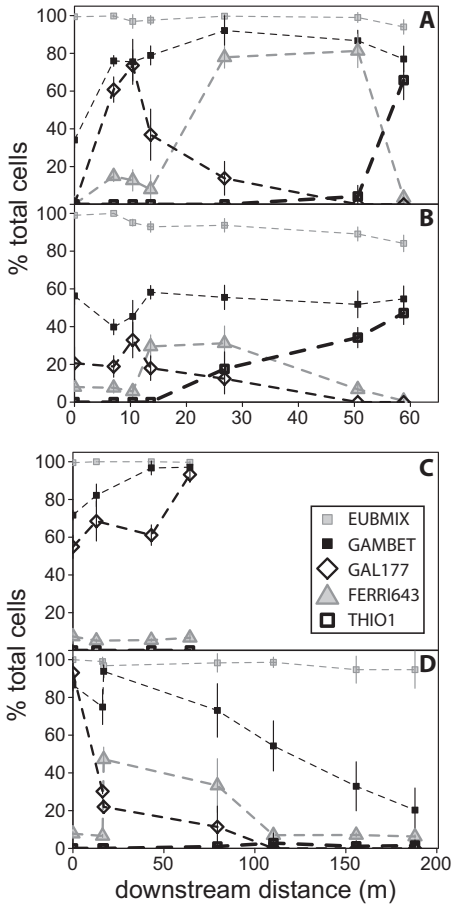

FIG 3 Changes in the relative abundances of microbial taxonomic groups as a function of distance from the AMD springs at Upper and Lower Red Eyes. Points represent the relative abundance of FISH-labeled cells (as a percentage of total DAPI-stained cells), and error bars represent 1 standard deviation. (A and B) Lower Red Eyes in April and October 2009, respectively. (C and D) Upper Red Eyes in January and April 2011, respectively. The abundances of FERRI643 and THIO1 in the panel A transect were reported previously (7). Representative FISH photomicrographs are shown in Fig. 4.

DISCUSSION

Microbial communities at Upper and Lower Red Eyes varied with distance downstream from the springs (Fig. 3). The microbial communities at each site also changed among sampling dates, as *Acidithiobacillus* became more abundant upstream at LRE in the fall than in the spring, and the distribution of *Gallionellaceae* at URE was expanded in January compared with that in April (Fig. 3). Dissimilarity among microbial communities was significantly correlated with dissimilarity among sites based on all environmental parameters (Mantel test, $r_M = 0.41$, $P = 0.001$) and based on pH and Fe^{2+} concentration alone (Mantel test, $r_M = 0.42$, $P = 0.001$). Ordination analyses revealed that the major axes of variance among the Red Eyes microbial communities corresponded to changes in pH, Fe^{3+}, Fe^{2+}, and p*e* (Fig. 5). The abundance of *Gallionellaceae* was positively correlated with pH and Fe^{2+} (Spearman's ρ: pH = 0.68, $P < 0.001$; Fe^{2+} = 0.63, $P < 0.001$), and that

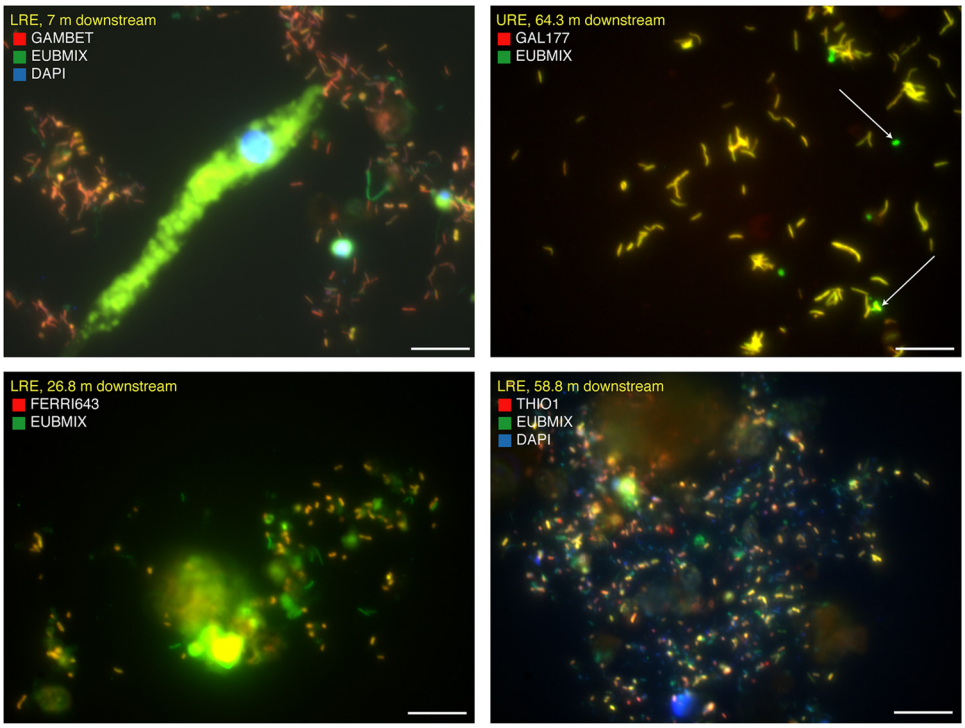

FIG 4 Representative fluorescence *in situ* hybridization (FISH) photomicrographs of microbial communities in Red Eyes sediments. A *Euglena* cell is pictured in the upper left image. Autofluorescence in the lower left image is likely due to the presence of extracellular polymeric substances. White arrows in the upper right image indicate cells that do not hybridize with probe GAL177.

of *Acidithiobacillus* was negatively correlated with pH and Fe^{2+} (Spearman's ρ: pH = −0.86, $P < 0.001$; Fe^{2+} = −0.76, $P < 0.001$). *Ferrovum* occurred at intermediate distances along stream transects and was not correlated with either (Spearman's ρ: pH = −0.04, $P = 0.81$; Fe^{2+} = 0.14, $P = 0.46$). At LRE, communities inhabiting terrace sediments were not statistically significantly different from communities inhabiting pool sediments (ANOSIM, $R = -0.13$, $P = 0.78$), which suggests that geochemical parameters affect the microbial community composition more than water flow velocity.

Because our sampling scheme effectively captured a wide range of pH, p*e*, and Fe conditions, we were able to resolve the effects of these individual parameters on microbial populations. We found that a combination of $[Fe^{2+}]$ and pH better explains the distribution of microbial communities than any single parameter. Figure 6 shows that the three most abundant populations at Red Eyes occupied niches with distinct $[Fe^{2+}]$ and pH values. *Gallionellaceae* were most abundant at locations with pH >3 and $[Fe^{2+}]$ of >4 mM, *Ferrovum* spp. predominated at sites with pH <3 and $[Fe^{2+}]$ of >4 mM, and *Acidithiobacillus* spp. were restricted to zones with pH <3 and $[Fe^{2+}]$ of <4 mM. pH alone does not explain the observed distribution of microbial populations. For example, both *Acidithiobacillus* and *Ferrovum* were abundant at pH values between 2.5 and 3, but *Acidithiobacillus* spp. were restricted to areas with lower $[Fe^{2+}]$. The appearance of *Acidithiobacillus* spp. further upstream at LRE in October than in April (cf. panels B and A in Fig. 3) corresponds to lower $[Fe^{2+}]$ in October (Fig. 1). Indeed, the absence of *Acidithiobacillus* spp. at Upper Red Eyes is likely because pH remains close to 3 even at the most downstream sites (Fig. 1). Likewise, the greater abundance of *Gallionellaceae* populations downstream at URE in January than in April corresponds to higher $[Fe^{2+}]$ in January. In a few samples, *Ferrovum* is abundant at pH >3 but low $[Fe^{2+}]$, which suggests that it may also dominate under those conditions (Fig. 6). However, further sampling will be required to describe the microbial communities that occur at pH >3 and low $[Fe^{2+}]$.

Our analyses also showed that pH is inversely correlated with $[Fe^{3+}]$ and that $[Fe^{2+}]$ is inversely correlated with p*e* (Fig. 5). This is likely because Fe oxide precipitation has a strong impact on pH (equation 4) and because Fe^{2+} oxidation (equation 3) controls the redox potential in the AMD spring outflows (see Fig. S1 in the supplemental material). Our results do not exclude the possibility that p*e*, Fe^{3+}, or other parameters may play a role in determining microbial distributions at other AMD sites. The Red Eyes springs have only minor variations in dissolved trace metal and phosphorus concentrations (7, 12), a characteristic which may have allowed us to isolate the effects of pH, p*e*, and Fe on microbial community composition. Globally, AMD discharges are complex environments that encompass a much wider range in temperature, pH, conductivity, metal concentrations, and other environmental parameters that are potentially important for defining microbial niches.

Our finding that pH and Fe^{2+} explain the distribution of microbial populations at the Red Eyes AMD springs is consistent with physiological studies of acidophilic iron oxidizers. Iron is the primary energy source for lithotrophs in AMD, and the relative proportion of Fe^{2+} and Fe^{3+} is thought to select for certain AMD populations (for an example, see reference 20). *Ferrovum* spp. occur in diverse AMD environments, including sites with extremely high $[Fe^{2+}]$, up to 71 mM (10). pH is widely considered an

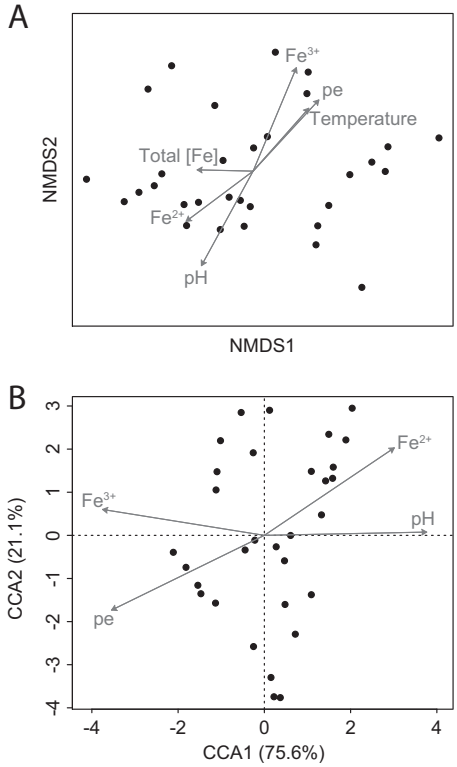

FIG 5 Nonmetric multidimensional scaling (NMDS) (A) and canonical correspondence analysis (CCA) ordinations (B) of Red Eyes microbial communities, based on FISH data. Points are sample scores, vectors in panel A are environmental variables overlain on the NMDS (stress = 0.10 for the NMDS ordination), and vectors in panel B are constraining variables in the CCA. Parenthetical values in panel B are the percentages of the total constrained variation explained by each axis. In total, 42.3% of total inertia is constrained in the CCA.

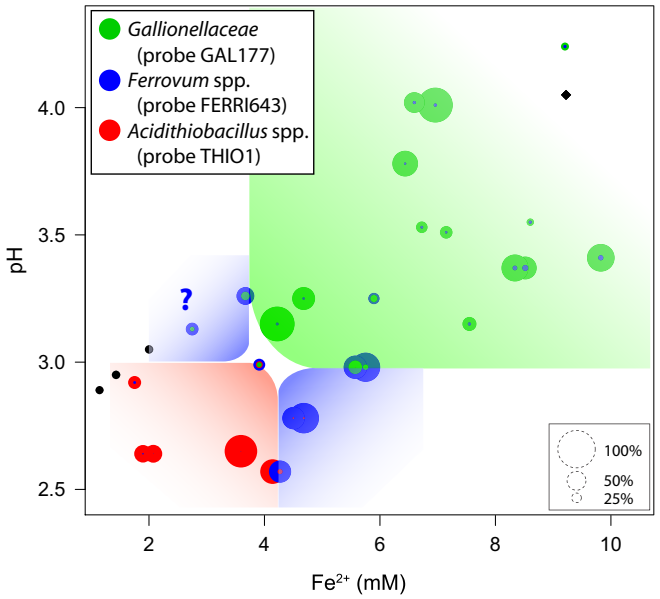

FIG 6 Distribution of *Ferrovum*, *Acidithiobacillus*, and *Gallionella*-like organisms with respect to Fe^{2+} concentration and pH. Points are scaled to the relative abundance of those organisms (as a percentage of total DAPI-stained cells). Black points indicate samples with <10% GAL177-, FERRI643-, and THIO1-hybridizing cells combined. Shaded regions indicate proposed niches for the respective organisms in the Red Eyes drainage. The question mark indicates a possible high-pH (>3) low-$[Fe^{2+}]$ niche for *Ferrovum*.

important variable in shaping AMD microbial communities, perhaps because it reflects or controls other geochemical parameters. Additionally, acidity is an environmental constraint that necessitates specific biological adaptations (48). Microbial acidophiles use a variety of mechanisms to lower membrane permeability to H^+ ions, including reversed membrane potential (49) and specialized membrane lipid structures (50, 51). pH also controls the aqueous speciation of Fe-SO_4 complexes that impact ferrihydrite or schwertmannite precipitation, which can impair cellular transport processes and impact the availability of Fe^{2+} to microbial cells (52). Multiple studies have noted the role of pH in partially explaining microbial community distribution in AMD (13–15). Interestingly, in a study of pilot scale iron oxidation bioreactors, a shift from *Ferrovum*- to *Gallionella*-dominated communities occurred with a slight increase in pH (to just above 3) and a slight decrease in Fe^{3+} during the late stages of operation of one reactor (46). This study is consistent with the niches occupied by *Ferrovum* and *Gallionella* at our study sites.

Our results have implications for low-pH iron oxidation as a bioremediation strategy. *Ferrovum* spp. have the highest specific iron oxidation rates of all strains reported measured in reference 53, and Hedrich and Johnson (6) showed that *Ferrovum* biofilms were especially effective in iron-oxidizing bioreactors. Indeed, in earlier work at LRE, *Ferrovum*-dominated sediment communities outperformed *Acidithiobacillus*-dominated communities in flow-through laboratory reactors (7). Little is known about the iron oxidation capabilities of the *Gallionellaceae*-dominated communities, but perhaps geochemical conditions could be manipulated in bioreactors or engineered treatment systems to preferentially select for *Ferrovum* over *Gallionellaceae* to maximize Fe oxidation rates or increase *Ferrovum* biomass. More generally, a systematic framework like that presented here (Fig. 6) could help to inform the design of future bioreactor and passive treatment systems and perhaps allow for the selection of particular microbial communities or even specific iron-oxidizing strains.

ACKNOWLEDGMENTS

We acknowledge the contributions of anonymous reviewers whose comments improved the manuscript.

This work was partially supported by the U.S. Office of Surface Mining Reclamation and Enforcement under Cooperative Agreement S11AC20005 and by NASA NAI (NNA04CC06A).

Special thanks to Linda Amaral-Zettler and Elizabeth McCliment for producing the rRNA gene pyrotag library. We thank Juliana Brown, Daniel Mills, Trinh DeSa, Irene Schaperdoth, and Stephanie McPherson for assistance in the field and laboratory. D. Barrie Johnson kindly provided a culture of *Ferrovum myxofaciens* for the development of our FISH probe. We thank Brent Means from the U.S. Office of Surface Mining and Malcolm Crittenden from the Pennsylvania Department of Environmental Protection for insightful discussions and for introducing us to the Red Eyes sites.

REFERENCES

1. **Herlihy AT, Kaufmann PR, Mitch ME, Brown DD.** 1990. Regional estimates of acid mine drainage impact on streams in the mid-Atlantic and southeastern United States. Water Air Soil Poll **50**:91–107.
2. **Hudson-Edwards KA, Jamieson HE, Lottermoser BG.** 2011. Mine

wastes: past, present, future. Elements **7:**375–380. http://dx.doi.org/10.2113/gselements.7.6.375.
3. **Tremblay G, Hogan C.** 2001. Mine environment neutral drainage (MEND) manual 5.4. 2d: prevention and control. Canada Centre for Mineral and Energy Technology, Natural Resources Canada, Ottawa, Canada.
4. **Johnson DB, Hallberg KB.** 2005. Acid mine drainage remediation options: a review. Sci Total Environ **338:**3–14. http://dx.doi.org/10.1016/j.scitotenv.2004.09.002.
5. **Burgos WD, Borch T, Troyer LD, Luan F, Larson LN, Brown JF, Lambson J, Shimizu M.** 2012. Schwertmannite and Fe oxides formed by biological low-pH Fe(II) oxidation versus abiotic neutralization: impact on trace metal sequestration. Geochim Cosmochim Acta **76:**29–44. http://dx.doi.org/10.1016/j.gca.2011.10.015.
6. **Hedrich S, Johnson DB.** 2012. A modular continuous flow reactor system for the selective bio-oxidation of iron and precipitation of schwertmannite from mine-impacted waters. Bioresour Technol **106:**44–49. http://dx.doi.org/10.1016/j.biortech.2011.11.130.
7. **Brown JF, Jones DS, Mills DB, Macalady JL, Burgos WD.** 2011. Application of a depositional facies model to an acid mine drainage site. Appl Environ Microbiol **77:**545–554. http://dx.doi.org/10.1128/AEM.01550-10.
8. **Singer PC, Stumm W.** 1970. Acidic mine drainage: the rate-determining step. Science **167:**1121–1123. http://dx.doi.org/10.1126/science.167.3921.1121.
9. **Johnson DB, Kanao T, Hedrich S.** 2012. Redox transformations of iron at extremely low pH: fundamental and applied aspects. Front Microbiol **3:**96. http://dx.doi.org/10.3389/fmicb.2012.00096.
10. **Johnson DB, Hallberg KB, Hedrich S.** 2014. Uncovering a microbial enigma: isolation and characterization of the streamer-generating, iron-oxidizing, acidophilic bacterium "*Ferrovum myxofaciens*."Appl Environ Microbiol **80:**672–680. http://dx.doi.org/10.1128/AEM.03230-13.
11. **Rowe OF, Johnson DB.** 2008. Comparison of ferric iron generation by different species of acidophilic bacteria immobilized in packed-bed reactors. Syst Appl Microbiol **31:**68–77. http://dx.doi.org/10.1016/j.syapm.2007.09.001.
12. **Larson LN, Sánchez-España J, Burgos W.** 2014. Rates of low-pH biological Fe(II) oxidation in the Appalachian Bituminous Coal Basin and the Iberian Pyrite Belt. Appl Geochem **47:**85–98. http://dx.doi.org/10.1016/j.apgeochem.2014.05.012.
13. **Baker BJ, Banfield JF.** 2003. Microbial communities in acid mine drainage. FEMS Microbiol Ecol **44:**139–152. http://dx.doi.org/10.1016/S0168-6496(03)00028-X.
14. **Lear G, Niyogi D, Harding J, Dong Y, Lewis G.** 2009. Biofilm bacterial community structure in streams affected by acid mine drainage. Appl Environ Microbiol **75:**3455–3460. http://dx.doi.org/10.1128/AEM.00274-09.
15. **Kuang J-L, Huang L-N, Chen L-X, Hua Z-S, Li S-J, Hu M, Li J-T, Shu W-S.** 2012. Contemporary environmental variation determines microbial diversity patterns in acid mine drainage. ISME J **7:**1038–1050. http://dx.doi.org/10.1038/ismej.2012.139.
16. **Edwards KJ, Gihring TM, Banfield JF.** 1999. Seasonal variations in microbial populations and environmental conditions in an extreme acid mine drainage environment. Appl Environ Microbiol **65:**3627–3632.
17. **Schrenk MO, Edwards KJ, Goodman RM, Hamers RJ, Banfield JF.** 1998. Distribution of *Thiobacillus ferrooxidans* and *Leptospirillum ferrooxidans*: implications for generation of acid mine drainage. Science **279:**1519. http://dx.doi.org/10.1126/science.279.5356.1519.
18. **Amaral-Zettler LA, Zettler ER, Theroux SM, Palacios C, Aguilera A, Amils R.** 2011. Microbial community structure across the tree of life in the extreme Rio Tinto. ISME J **5:**42–50. http://dx.doi.org/10.1038/ismej.2010.101.
19. **Palacios C, Zettler E, Amils R, Amaral-Zettler L.** 2008. Contrasting microbial community assembly hypotheses: a reconciling tale from the Rio Tinto. PLoS One **3:**e3853. http://dx.doi.org/10.1371/journal.pone.0003853.
20. **Rawlings D, Tributsch H, Hansford G.** 1999. Reasons why '*Leptospirillum*'-like species rather than *Thiobacillus ferrooxidans* are the dominant iron-oxidizing bacteria in many commercial processes for the biooxidation of pyrite and related ores. Microbiology **145:**5–13. http://dx.doi.org/10.1099/13500872-145-1-5.
21. **Martiny JBH, Bohannan BJM, Brown JH, Colwell RK, Fuhrman JA, Green JL, Horner-Devine MC, Kane M, Krumins JA, Kuske CR.** 2006. Microbial biogeography: putting microorganisms on the map. Nat Rev Microbiol **4:**102–112. http://dx.doi.org/10.1038/nrmicro1341.
22. **Macalady JL, Jones DS, Lyon EH.** 2007. Extremely acidic, pendulous microbial biofilms from the Frasassi cave system, Italy. Environ Microbiol **9:**1402–1414. http://dx.doi.org/10.1111/j.1462-2920.2007.01256.x.
23. **Stookey LL.** 1970. Ferrozine—a new spectrophotometric reagent for iron. Anal Chem **42:**779–781. http://dx.doi.org/10.1021/ac60289a016.
24. **Bourrié G, Trolard F, Jaffrezic J-MRG, Maître V, Abdelmoula M.** 1999. Iron control by equilibria between hydroxy-green rusts and solutions in hydromorphic soils. Geochim Cosmochim Acta **63:**3417–3427. http://dx.doi.org/10.1016/S0016-7037(99)00262-8.
25. **Stumm W, Morgan J.** 1996. Aquatic chemistry, 3rd ed, p 1040. Wiley, New York, NY.
26. **Bethke CM.** 2010. Geochemical and biogeochemical reaction modeling, 2nd ed. Cambridge University Press, Cambridge, United Kingdom.
27. **Larson LN, Sánchez-España J, Kaley B, Sheng Y, Bibby K, Burgos WD.** 2014. Thermodynamic controls on the kinetics of microbial low-pH Fe(II) oxidation. Environ Sci Technol **48:**9246–9254. http://dx.doi.org/10.1021/es501322d.
28. **Macalady JL, Dattagupta S, Schaperdoth I, Jones DS, Druschel GK, Eastman D.** 2008. Niche differentiation among sulfur-oxidizing bacterial populations in cave waters. ISME J **2:**509–601. http://dx.doi.org/10.1038/ismej.2008.25.
29. **Senko JM, Wanjugi P, Lucas M, Bruns MA, Burgos WD.** 2008. Characterization of Fe(II) oxidizing bacterial activities and communities at two acidic Appalachian coalmine drainage-impacted sites. ISME J **2:**1134–1145. http://dx.doi.org/10.1038/ismej.2008.60.
30. **McCliment EA, Nelson CE, Carlson CA, Alldredge AL, Witting J, Amaral-Zettler LA.** 2012. An all-taxon microbial inventory of the Moorea coral reef ecosystem. ISME J **6:**309–319. http://dx.doi.org/10.1038/ismej.2011.108.
31. **Hugenholtz P, Tyson G, Blackall L.** 2002. Design and evaluation of 16S rRNA-targeted oligonucleotide probes for fluorescence *in situ* hybridization. Methods Mol Biol **179:**29–42. http://dx.doi.org/10.1385/1-59259-238-4:029.
32. **Yeates C, Saunders AM, Crocetti GR, Blackall LL.** 2003. Limitations of the widely used GAM42a and BET42a probes targeting bacteria in the *Gammaproteobacteria* radiation. Microbiology **149:**1239–1247. http://dx.doi.org/10.1099/mic.0.26112-0.
33. **Pruesse E, Quast C, Knittel K, Fuchs BM, Ludwig W, Peplies J, Glöckner FO.** 2007. SILVA: a comprehensive online resource for quality checked and aligned ribosomal RNA sequence data compatible with ARB. Nucleic Acids Res **35:**7188–7196. http://dx.doi.org/10.1093/nar/gkm864.
34. **Williams KP, Kelly DP.** 2013. Proposal for a new class within the phylum *Proteobacteria*, *Acidithiobacillia* classis nov., with the type order *Acidithiobacillales*, and emended description of the class *Gammaproteobacteria*. Int J Syst Evol Microbiol **63:**2901–2906. http://dx.doi.org/10.1099/ijs.0.049270-0.
35. **DeSantis TZ, Hugenholtz P, Larsen N, Rojas M, Brodie EL, Keller K, Huber T, Dalevi D, Hu P, Andersen GL.** 2006. Greengenes, a chimera-checked 16S rRNA gene database and workbench compatible with ARB. Appl Environ Microbiol **72:**5069–5072. http://dx.doi.org/10.1128/AEM.03006-05.
36. **Huber T, Faulkner G, Hugenholtz P.** 2004. Bellerophon: a program to detect chimeric sequences in multiple sequence alignments. Bioinformatics **20:**2317–2319. http://dx.doi.org/10.1093/bioinformatics/bth226.
37. **Ludwig W, Strunk O, Westram R, Richter L, Meier H, Yadhukumar Buchner A, Lai T, Steppi S, Jobb G, Förster W, Brettske I, Gerber S, Ginhart AW, Gross O, Grumann S, Hermann S, Jost R, König A, Liss T, Lüßmann R, May M, Nonhoff B, Reichel B, Strehlow R, Stamatakis A, Stuckmann N, Vilbig A, Lenke M, Ludwig T, Bode A, Schleifer K-H.** 2004. ARB: a software environment for sequence data. Nucleic Acids Res **32:**1363–1371. http://dx.doi.org/10.1093/nar/gkh293.
38. **Swofford DL.** 2000. PAUP*: phylogenetic analysis using parsimony and other methods. Sinauer Associates, Sunderland, MA.
39. **Huse SM, Dethlefsen L, Huber JA, Welch DM, Relman DA, Sogin ML.** 2008. Exploring microbial diversity and taxonomy using SSU rRNA hypervariable tag sequencing. PLoS Genet. **4:**e1000255. http://dx.doi.org/10.1371/journal.pgen.1000255.
40. **Schloss PD, Westcott SL, Ryabin T, Hall JR, Hartmann M, Hollister EB, Lesniewski RA, Oakley BB, Parks DH, Robinson CJ.** 2009. Introducing mothur: open-source, platform-independent, community-supported software for describing and comparing microbial communities. Appl Environ Microbiol **75:**7537–7541. http://dx.doi.org/10.1128/AEM.01541-09.

41. **Altschul SF, Madden TL, Schäffer AA, Zhang J, Zhang Z, Miller W, Lipman DJ.** 1997. Gapped BLAST and PSI-BLAST: a new generation of protein database search programs. Nucleic Acids Res **25:**3389–3402. http://dx.doi.org/10.1093/nar/25.17.3389.
42. **Oksanen J, Kindt R, Legendre P, O'Hara R, Simpson GL, Stevens MHH.** 2008. Vegan: community ecology package, R package version 1.11-0. http://cran.r-project.org/web/packages/vegan/index.html.
43. **R Core Development Team.** 2007. R: a language and environment for statistical computing. R Foundation for Statistical Computing, Vienna, Austria.
44. **McCune B, Grace JB.** 2002. Analysis of ecological communities. MjM Software Design, Gleneden Beach, OR.
45. **Hallberg KB, Coupland K, Kimura S, Johnson DB.** 2006. Macroscopic streamer growths in acidic, metal-rich mine waters in North Wales consist of novel and remarkably simple bacterial communities. Appl Environ Microbiol **72:**2022–2030. http://dx.doi.org/10.1128/AEM.72.3.2022-2030.2006.
46. **Heinzel E, Janneck E, Glombitza F, Schlömann M, Seifert J.** 2009. Population dynamics of iron-oxidizing communities in pilot plants for the treatment of acid mine waters. Environ Sci Technol **43:**6138–6144. http://dx.doi.org/10.1021/es900067d.
47. **Emerson D, Fleming EJ, McBeth JM.** 2010. Iron-oxidizing bacteria: an environmental and genomic perspective. Annu Rev Microbiol **64:**561–583. http://dx.doi.org/10.1146/annurev.micro.112408.134208.
48. **Baker-Austin C, Dopson M.** 2007. Life in acid: pH homeostasis in acidophiles. Trends Microbiol **15:**165–171. http://dx.doi.org/10.1016/j.tim.2007.02.005.
49. **Cox JC, Nicholls DG, Ingledew W.** 1979. Transmembrane electrical potential and transmembrane pH gradient in the acidophile *Thiobacillus ferro-oxidans*. Biochem J **178:**195–200.
50. **Macalady JL, Vestling MM, Baumler D, Boekelheide N, Kaspar CW, Banfield JF.** 2004. Tetraether-linked membrane monolayers in *Ferroplasma* spp.: a key to survival in acid. Extremophiles **8:**411–419. http://dx.doi.org/10.1007/s00792-004-0404-5.
51. **Welander PV, Hunter RC, Zhang L, Sessions AL, Summons RE, Newman DK.** 2009. Hopanoids play a role in membrane integrity and pH homeostasis in *Rhodopseudomonas palustris* TIE-1. J Bacteriol **191:**6145–6156. http://dx.doi.org/10.1128/JB.00460-09.
52. **Meruane G, Vargas T.** 2003. Bacterial oxidation of ferrous iron by *Acidithiobacillus ferrooxidans* in the pH range 2.5–7.0. Hydrometallurgy **71:**149–158. http://dx.doi.org/10.1016/S0304-386X(03)00151-8.
53. **Hedrich S, Schlömann M, Johnson DB.** 2011. The iron-oxidizing proteobacteria. Microbiology **157:**1551–1564. http://dx.doi.org/10.1099/mic.0.045344-0.
54. **Amann R, Binder BJ, Olson RJ, Chisholm SW, Devereux R, Stahl DA.** 1990. Combination of 16S rRNA-targeted oligonucleotide probes with flow cytometry for analyzing mixed microbial populations. Appl Environ Microbiol **56:**1919–1925.
55. **Daims H, Brühl A, Amann R, Schleifer K-H, Wagner M.** 1999. The domain-specific probe EUB338 is insufficient for the detection of all *Bacteria*: development and evaluation of a more comprehensive probe set. Syst Appl Microbiol **22:**434–444. http://dx.doi.org/10.1016/S0723-2020(99)80053-8.
56. **Stahl DA, Amann R.** 1991. Development and application of nucleic acid probes, p 205–248. *In* Stackebrandt E, Goodfellow M (ed), Nucleic acid techniques in bacterial systematics. John Wiley & Sons Ltd., Chichester, England.
57. **González-Toril E, Llobet-Brossa E, Casamayor E, Amann R, Amils R.** 2003. Microbial ecology of an extreme acidic environment, the Tinto River. Appl Environ Microbiol **69:**4853. http://dx.doi.org/10.1128/AEM.69.8.4853-4865.2003.
58. **Bond P, Banfield J.** 2001. Design and performance of rRNA targeted oligonucleotide probes for *in situ* detection and phylogenetic identification of microorganisms inhabiting acid mine drainage environments. Microb Ecol **41:**149–161. http://dx.doi.org/10.1007/s002480000063.
59. **Manz W, Amann R, Ludwig W, Wagner M, Schleifer K-H.** 1992. Phylogenetic oligodeoxynucleotide probes for the major subclasses of Proteobacteria: problems and solutions. Syst Appl Microbiol **15:**593–600. http://dx.doi.org/10.1016/S0723-2020(11)80121-9.